ON-SKY EVALUATION OF PASSIVE POLARIMETRY AS A TECHNIQUE TO CHARACTERISE SPACE DEBRIS

Manuel Cegarra Polo[(1)], Israel Vaughn[(2)], Andrey Alenin[(3)], Andrew Lambert[(4)]

(1) School of Engineering and IT, UNSW Canberra, Northcott Dr. Campbell, 2612, Canberra, ACT, Australia
Email: [(1)]m.cegarrapolo@adfa.edu.au
[(2)]i.vaughn@adfa.edu.au
[(3)]a.alenin@adfa.edu.au
[(4)]A-Lambert@adfa.edu.au

ABSTRACT

A combination of radar and optical observations is the current approach to track and classify space debris population with a size of 10 cm and above, but still there are opportunities for innovative techniques that can complement current observation procedures. Here, we propose the use of polarimetric information coming from passively solar illuminated space debris, to characterise these objects in a more comprehensive way.

To evaluate this technique, we began a preliminary study of a set of relatively bright space debris objects, rocket bodies, from different manufacturers and launching dates. Polarimetric signatures of these rocket bodies are compared with Low Earth Orbit (LEO) and Geostationary Equatorial Orbit (GEO) satellites, in order to analyse polarimetric information reflected from Resident Space Objects (RSO) with different shapes: cylindrical such as rocket bodies, and structures including solar panels, such as satellites.

1 INTRODUCTION

Different techniques are used to study the optical signatures created by the reflected light of passively sun-lit RSO, including irradiance, spectra or polarimetric measurements. Light curves obtained through irradiance-only optical signatures have been used for many years, and they can provide useful information to detect spinning rates of tumbling RSO [1]. Spectral data can be used to characterise RSO surfaces through wavelength-dependant material information [2]. However, as some authors stated [3], the use of polarisation information is an underused technique.

Polarimetry has showed utility in detecting geometry and material characteristics with resolved images for classification [4], but there are few studies characterising its use with unresolved images of passively solar illuminated RSO. These studies encompass computer-aided simulations [5], characterization of materials in a laboratory environment [6], and on-sky experimental results [7].

New and challenging issues arise with this application, such as the presence of a turbulent atmosphere along the light path, the light curve response in the case of tumbling space debris and satellites, the unresolved imagery in the sensor, the strong uncertainty of the predicted orbit due to unknown object shape which complicates its optical tracking, or the reduced photon count captured in the image sensors due to trade-off with temporal precision.

Polarimetric signatures in RSO depend on the type of material being imaged and the angle of incidence with the Sun. These signatures can potentially provide information about the surface microstructure and material composition, which in turn could be useful to deduce geometrical attitude, tumbling status and period, or type and aging of RSO materials.

Moreover, previous information could lead to an improvement in the accuracy of the predicted orbit through better astrodynamics models and to the reduction of debris and satellite cross-tagging due to misled optical identification of RSO.

2 POLARISATION BY REFLECTION

One of the ways that unpolarised light, like that coming from the Sun, transforms to polarised light, is by reflection. Provided that the incident surface is dielectric, we should obtain some degree of polarisation in the reflected light. The degree of polarisation will depend upon the incidence angle and the particular surface material.

Fig. 1 shows an incident light beam in a flat dielectric surface, where I_o and I are the incident and reflected beams associated intensities, n_1 and n_2 the refraction indexes, and i and r the angles with respect to the vector perpendicular to the surface in the incidence point.

Eq.1 can be deduced from Fresnel expressions [8],

$$\frac{I}{I_0} = \frac{sin^2(i-r)}{2sin^2(i+r)} + \frac{tan^2(i-r)}{2tan^2(i+r)} \qquad (1)$$

If the angle of the incident beam is such that $i + r = 90°$, the second term in Eq. 1 is zero, and the reflected light is completely plane polarized in the plane of incidence

(i.e., plane of the paper), that is, the reflected light is formed just by the component of the electric field vector perpendicular to the plane of incidence, which corresponds with the first term in Eq. 1 [8].

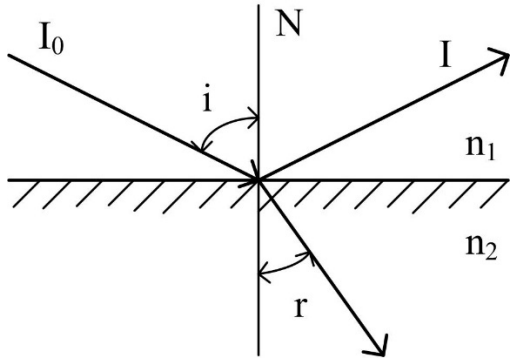

Figure 1. Unpolarised light incidence in dielectric surface.

According to Snell's equation:

$$\frac{sin\ i}{sin\ r} = \frac{n_1}{n_2} = n_{12} \quad (2)$$

If $i + r = 90°$, Eq. 2 becomes:

$$\frac{sin\ i_b}{cos\ i_b} = \tan i_b = n_{12} \quad (3)$$

where i_b is the polarizing or Brewster angle, and all light reflected at this angle will be one hundred percent polarised in the plane of incidence.

In the case of RSO, typically solar panels or glossy painting are dielectric surfaces, so we should expect to obtain certain degree of polarisation from them, while pure metallic surfaces shouldn't show any polarised component normal to the surface, however surface geometry can also induce polarisation.

This means that in the case of a RSO, there should be favourable phase angles (angle at the RSO subtended by the observer and the Sun), where polarisation by reflection would be maximized.

Such could be tested in a controlled experiment in laboratory, but with on-sky observations of RSO in motion, there are many other factors that can influence in the reflected polarized components, as slant range, air mass, atmosphere turbulence, size and attitude of the object, area of the incident light over the image sensor, alignment of optical components in the sensor, tracking accuracy of the telescope mount, and so on.

3 EXPERIMENTAL SETUP

Observations have been accomplished with a Meade LX200EMC Classic telescope, with 0.3 metre aperture. A focal reducer was included in the optical train, in order to extend the original Field of View (FOV). Tab. 1 shows the more important features of the different elements of the optical setup.

Table 1. Main characteristics of optical elements.

Telescope Meade LX200 EMC	
Clear aperture	304.8 mm (12")
Focal length	3048 mm
Focal ratio	f/10
Resolution	0.375 arc sec
Mount	Alt-azimuth
Focal Reducer	Achromatic doublet F50
Camera 4D Technology	
Sensor	CCD ONSEMI KAI-1010
Spectral range	370 nm – 1000 nm
Pixel size	9 x 9 µm
Active image size	9.1 mm (H) x 9.2 mm (V)
Min. usable pixels	1008 (H) x 1018 (V)

A polarimetric camera, manufactured by 4D Technology, was used to measure the polarisation characteristics of the reflected light of RSO. This camera is formed by a micropolariser array bonded to the image sensor, which allows the camera to obtain polarisation parameters as a snapshot system.

Fig. 2 shows the optical setup used to collect the observations. The LX200 Classic is an F/10 Schmidt-Cassegrain telescope. The focal reducer, is an achromatic doublet from Thorlabs, with focal length 50 mm, and visible coating. The focal reducer is situated as close as possible to the back rear port of the telescope, in order the reduce vignetting.

The focal reducer, which increases the original FOV by a factor of 2.5, was found to be enough to compensate telescope alignment and tracking errors, Two Line Element (TLE) and orbit prediction errors. This eases the tracking of the RSO, in order to keep them within the limits of the image sensor during the acquiring time of the RSO pass.

Due to the internal structure of the micropolariser array in the image sensor, a minimum number of pixels with light coming from the RSO are needed, so the polarisation parameters are accurate. To accomplish this

task we utilised slightly defocused images. An example is represented in Fig. 2 by red light rays (unfocused) and blue light rays (focused).

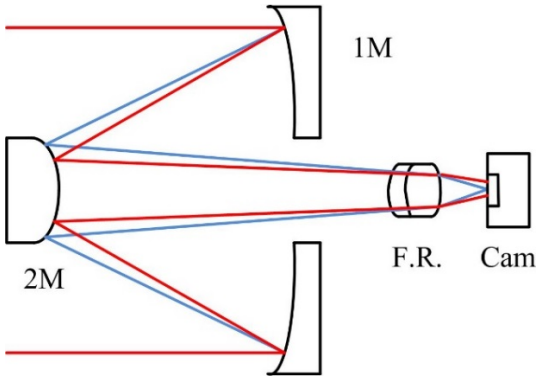

Figure 2. Optical setup: 1M (primary mirror), 2M (secondary mirror), F.R. (Focal Reducer) and Cam (polarimetric camera).

Fig. 3 shows an example of unfocused images obtained on the image sensor, where the obscuration produced by the secondary mirror of the telescope can be appreciated in the image.

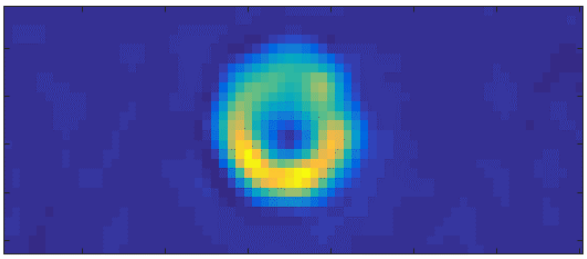

Figure 3. Unfocused image of GEO satellite NORAD 37737.

There is a trade-off between the number of pixels in the unfocused region, and the intensity level per pixel. In order to make the camera work in its linear range we defocused the image and above the noise level so that 5 to 20 pixels were illuminated.

The proposed RSO targets have high values of relative magnitude, with maximum values ranging between 4 and 6 (in the perigee and 100% illuminated).

For this magnitude, 0.8 seconds of integration time was found to be a good compromise value for LEO objects (rocket bodies and satellites) for the proposed object orbits, while a value of 3.2 seconds of integration time was chosen for the GEO satellites, due to the high slant range of these satellites.

3.1 Telescope

The telescope is an amateur class Meade LX200 EMC Classic model. The optical tube is assembled in a computerized mount in alt-azimuthal mode.

The magnification (f/10) of the telescope provides a relatively small FOV in the image sensor (8 x 7 arc min), which was found not to be sufficient to maintain the tracked LEO objects within the FOV. For this reason, a focal reducer was inserted in the optical train close to the rear port of the telescope in order to increase the FOV to a size of 20 x 18 arc min.

Errors in the tracking are introduced by the TLE and SGP4 propagation algorithm uncertainties, and by the alignment, mechanical and periodic errors in the mount of the telescope. With the extended FOV provided by the focal reducer, all proposed targets were within the FOV.

3.2 Polarimetric camera

The science camera is a 4D Technology camera which consists of a CCD sensor (ONSEMI KAI-1010) bonded to a micropolariser array, proprietary technology of the manufacturer.

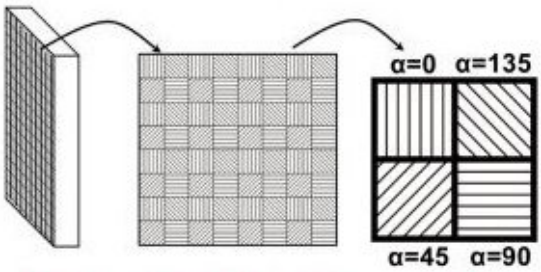

Figure 4. Internal structure of polarimetric camera: camera sensor (left), polarizer array (centre), unit cell (right). Image credit: www.4dtechnology.com.

With this technology, four polarisation angles can be acquired simultaneously with just one image sensor (See fig. 4).

The advantage of this camera compared to other methods to extract polarimetric information, is that the S0, S1 and S2 measurements are obtained directly on the camera with no temporal modulation necessary. Other techniques as the use of polarizing beamsplitters or rotating linear polarizers, requires further processing and are more prone to errors due to optical misalignments in the optical train.

Additionally, because only one camera is used, we don't need to calibrate different cameras, as is the case of polarizing beamsplitters.

4 OBSERVATIONS

As a test to characterize space debris objects through polarimetry, a set of bright objects, rocket bodies, was chosen as targets. Particularly three rocket bodies (NORAD 694, 20775 and 21820), one LEO satellite (NORAD 23087) and one GEO satellite (NORAD 37737). In Tab. 2 the main characteristics of these RSO are shown, together with the acquired number of frames, the exposure time and the number of frames per seconds used in the camera.

In Fig. 5 are shown the passes of each imaged rocket body and satellite, with the coloured lines indicating the section of the passes were images were acquired.

Table 2. List of main characteristics of observed RSO.

NORAD	Name	Type	Orbit	Model	Launch date	Size (m)	Frames	fps	Exp (ms)
694	Atlas Centaur	R/B	LEO	D stage	27-11-1963	3x21x5	120	1	800
20775	SL-8 R/B	R/B	LEO	11K65M	28-08-1990	2.4x6x4.4	120	1	800
21820	SL-14 R/B	R/B	LEO	Tsiklon-3	18-12-1991	2.25x2.58	240	1	800
23087	Cosmos 2278	Satellite	LEO	Tselina-2	23-04-1994	-	60	1	800
37737	Tianlian 1-02	Satellite	GEO	Chang	11-07-2011	2x1.7x2 Span 18m	380	0.2	3200

Passes of rocket bodies 694 and 20775 are at Northwest, 21820 rocket body in Southwest, 23087 LEO satellite in South, and 37737 GEO satellite is in an area surrounding Alt=37º AZ=40º coordinates.

All acquired section of passes are short in time and relatively low above the horizon, in order to reduce the influence of the slant range and air mass.

Tab. 3 shows the Sun height angle and time run for each RSO, which is related with the phase angle during the time of observation.

In these observations, we will measure S0 and DoLP. S0 S0 is the ensemble average of the *Ex* and *Ey* electrical field components and it corresponds to the integrated Poynting vector:

$$S0 =< E_x E_x^* > +< E_y E_y^* > \qquad (4)$$

DoLP is the degree of linear polarisation and is defined as:

$$DoLP = \sqrt{(S_1^2 + S_2^2)/S0} \qquad (5)$$

Where S1 and S2 describes linear polarisation along *x* or *y* axis, and along direction at angles ±45º to the *x* axis respectively.

Table 3.Time of observation runs and Sun height angle (credit: www.heavens-above.com).

NORAD	Time	Sun h. min	Sun h. max
694	2 min	-37.7º	-39.2º
20775	1+1 min	-23.9º	-24.7º
21820	2+2 min	-28.7º	-31.1º
23087	1 min	-34.0º	-34.2º
37737	20 min	-	-

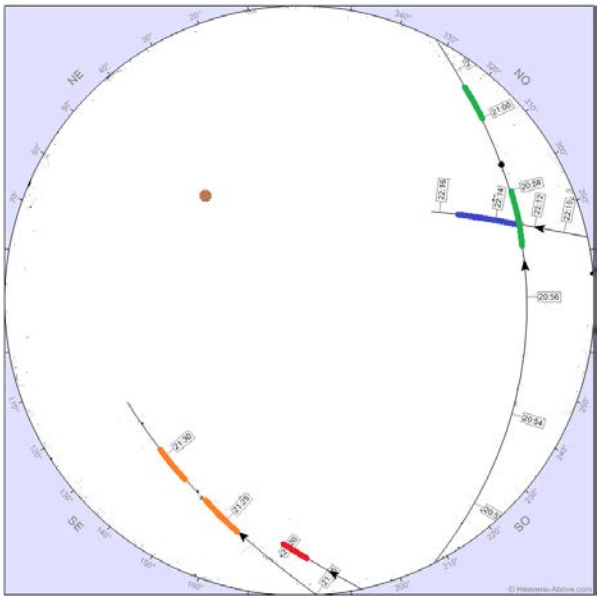

Figure 5. Passes of the studied RSO: 694(blue), 20775(green), 21820(orange), 23087(red), 37737(brown). (credit: www.heavens-above.com)

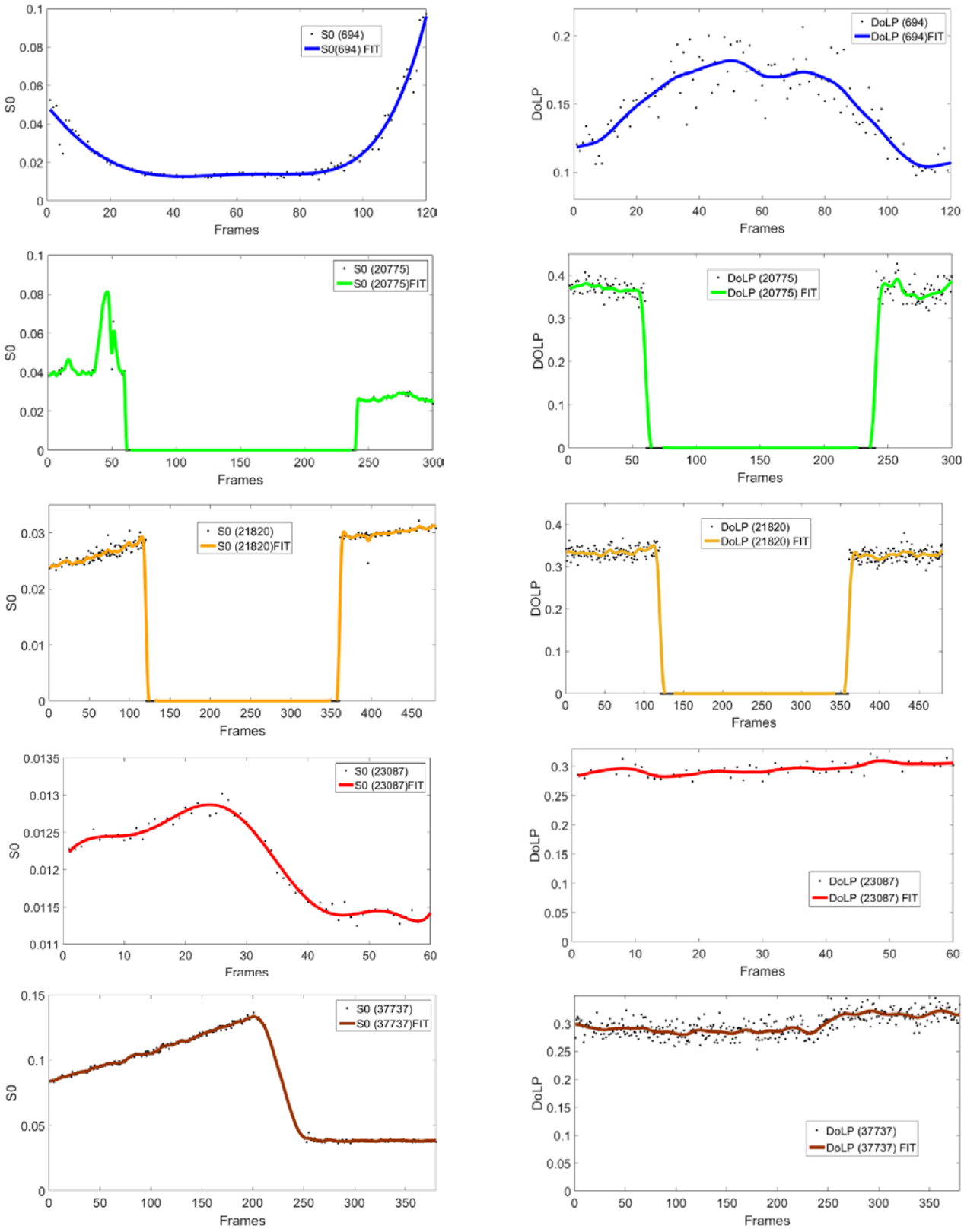

Figure 6. S_0 (left) and DoLP (right) of each RSO.

5 RESULTS

Fig. 6 shows the light curves from S0 and DoLP for each of the five RSO under study, being S0 the integrated irradiance (equivalent to what image sensor would detect without the micropolariser array), and DoLP the fraction of the incident beam which is linearly polarised. Both quantities are calibrated using a sensor acquired for a 5 ms exposure time.

In this figure, S0 curves are shown in the left part and DoLP in the right, following the same colour code as in Fig. 5.

In the horizontal axis of each figure is represented the number of frames, which in the first four RSO is also the time length of the observation in seconds, because frame rate is 1 fps. In the last RSO (37737) the value of the frame rate is 0.2 fps.

In order to observe the trend in the curves more easily, data have been fitted to smooth splines, except in the case of the RSO 694, which was fitted with a polynomial curve of degree 5.

From the observation of these curves, some aspects can be highlighted:

- S0 curves shows 2 tumbling rocket bodies (694 and 20775), one steady rocket body (21820), a LEO satellite (23087) with a small variation in intensity, and a GEO satellite (37737) that enters in the shadow of the Earth (eclipsed) from frame 200 to 250 approximately.
- DoLP curves shows in general low values with low variability, around 0.3-0.4, except for the object 694. We suspect that the constant relatively high DoLP level is a systematic error.

Object 694 was launched in 1963, while the rest were launched at least 27 years after, or more recently. The degradation in the external coating in this object could explain the lower value in DoLP, compared to the rest. Historical documentation on 694 suggests that the rocket body has a large layer of foam.

Interestingly, DoLP increases when the object 694 reflect less light, which suggest that during that period, we are receiving the light reflected from first surface reflection, rather than volumetric scattering and reflection.

Object 20775 shows a relatively high tumbling rate, noted by the two peaks in the left part of figure, but the DoLP is almost constant, around 0.39. In the right part of the acquisitions, we again observe the same effect that with the 694 object (increase of DoLP when S0 decreases and vice versa), but less evident.

Curve of RSO 21820 is almost steady during the acquisition period, which indicates that the object is reflecting light with almost the same attitude towards us. There are no significant variations in the DoLP, probably due to the fact that we are looking at the same surface during the acquisition period.

In the case of the satellites, LEO (23087) and GEO (37737), DoLP is almost constant, despite variations in the S0 curves. This suggests that, if there is tumbling or spinning, a symmetry axis is involved, or that the true DoLP is hidden by the likely systematic error.

6 CONCLUSIONS

We have conducted preliminary studies on RSO consisting in rocket bodies, LEO and GEO satellites using a polarimetric camera with an amateur class telescope LX200 EMC 0.3 metres aperture. DoLP and S0 have been measured directly with an image sensor which includes a micropolariser array.

Results from these tests indicate that there may be different polarisation degrees depending of launch date of the RSO, and therefore, possibly indicating degradation of their surfaces, however further calibration is needed to remove systematic errors.

Polarisation measurements add extra information to the irradiance only light curves, and they can indicate what type of surface (dielectric or metallic) is reflecting the light between peaks in tumbling pieces of space debris or satellites.

These results show a promising path to follow, but still require further investigation extending the type of observed object and the duration of the acquired section of the pass, which could confirm if same trends are observed in other RSO.

7 REFERENCES

1. J. G. Williams & G.A. McCue (1966). An Analysis of Satellite Optical Characteristics Data. In *Planet. Space Sci.*, Vol. 14, pp. 839 to 847. Pergamon Press Ltd.
2. John V. Lambert (1971). Measurement of the Visible Spectra of Orbiting Satellites. *Thesis presented to the Faculty of the School of Engineering of the Air Force Institute of Technology Air University*.
3. Scott Tyo J., Goldstein L., Chenaut D.B. & Shaw J.A. (2006). Review of passive imaging polarimetry for remote sensing applications. In *Applied Optics*, Vol. 45, No. 22.
4. Israel J. Vaughn, Brian G. Hoover & J. Scott Tyo (2012). Classification using active polarimetry. In *Proceedings SPIE*, vol. 8364, 83640S.
5. Stryjewski J. et al. (2010). Real Time Polarisation Light Curves for Space Debris and Satellites. In *Proc. AMOS Conference.* Hawaii, US.

6. Pasqual M.C., Kahoi K.L. & Hines E.L. (2015). Active Polarimetry for Orbital Debris Identification. In *Proc. AMOS Conference.* Hawaii, US.

7. A. Speicher, M. Matin, R.D. Tippets, F.K. Chun & D. Strong (2015). Results from an experiment that collected visible-light polarisation data using unresolved imagery for classification of geosynchronous satellites. In *Proceedings SPIE*, vol. 9460, p. 946006.

8. Richard Patton Stead (1967). An Investigation of Polarisation Phenomena produced by Space Objects. *Thesis presented to the Faculty of the School of Engineering of the Air Force Institute of Technology Air University.*